

High-pressure Raman study of the alkaline-earth metal fulleride, $\text{Ca}_{2.75}\text{C}_{60}$

A. G. V. Terzidou*, T. Nakagawa†, N. Yoshikane‡, R. Rountou*, J. Rix*·§, O. Karabinaki¶, D. Christofilos¶, J. Arvanitidis*·** and K. Prassides‡,||,††

* *Physics Department, Aristotle University of Thessaloniki,
54124 Thessaloniki, Greece*

† *Center for High-Pressure Science & Technology Advanced Research,
100094 Beijing, P. R. China*

‡ *Department of Materials Science, Graduate School of Engineering,
Osaka Prefecture University, 599-8531 Osaka, Japan*

§ *Freiberg University of Mining and Technology, Institute of Theoretical Physics,
Leipziger Straße 23, 09599 Freiberg, Germany*

¶ *School of Chemical Engineering & Laboratory of Physics,
Faculty of Engineering, Aristotle University of Thessaloniki,
54124 Thessaloniki, Greece*

|| *Advanced Institute for Materials Research (WPI-AIMR),
Tohoku University, Sendai 980-8577, Japan*

** *jarvan@physics.auth.gr*

†† *k.prassides@mtr.osakafu-u.ac.jp*

HPSTAR
999-2020

Received 7 February 2020

Accepted 20 March 2020

Published 12 June 2020

The structural stability and electronic properties of $\text{Ca}_{2.75}\text{C}_{60}$ are probed by means of high-pressure Raman spectroscopy using two different pressure transmitting media that lead to practically identical results. Although $\text{Ca}_{2.75}\text{C}_{60}$ is isostructural with the rare-earth metal fulleride, $\text{Sm}_{2.75}\text{C}_{60}$ of the same stoichiometry, the pressure coefficients of characteristic intramolecular C_{60} modes are larger than those in the $\text{Sm}_{2.75}\text{C}_{60}$ counterpart but similar to those in the pristine C_{60} solid. Since the reduced pressure coefficients in the Sm fulleride have been attributed to strong Sm- C_{60} coupling, our findings for the isostructural Ca fulleride are compatible with a reduced orbital mixing and Ca- C_{60} coupling.

Keywords: Fullerides; strongly correlated electron systems; Raman spectroscopy; high pressure.

PACS Number(s): 78.30.Na, 62.50.-p, 61.48.-c, 71.27.+a

†† Corresponding author.

1. Introduction

Alkaline (AE) and rare-earth (RE) metal C_{60} fullerides — metal intercalation compounds of C_{60} — comprise an interesting class of novel, highly correlated molecular systems due to the possible strong orbital mixing between the metal atom and the C_{60} π electron states.¹ RE fullerides (RE = Sm, Eu, Yb) adopt a stable $RE_{2.75}C_{60}$ stoichiometry and form an orthorhombic superstructure with dimensions twice as large as those of A_3C_{60} (A = alkali metal) in every direction due to the ordering of partially occupied tetrahedral cation defects.² Owing to the fragility of the valence state of the rare-earth ions and the presence of the also electronically active anion (C_{60}) sublattice,^{3–5,32} these systems exhibit on cooling an isosymmetric phase transition accompanied by a dramatic anomalous isotropic volume increase caused by the rare-earth valence transition from a mixed valence $(2 + \varepsilon) + (0 < \varepsilon < 1)$ state to nearly $2+$.^{2,6} This effect was unprecedented in molecular systems and is reminiscent of the valence transitions encountered in intermediate valence Kondo insulators like SmS, which undergo pressure-induced abrupt transitions from a semiconducting black to a metallic gold phase.⁵ Indeed, $Sm_{2.75}C_{60}$ also shows a huge pressure-induced lattice collapse and changes in its optical properties at ~ 4 GPa, implying an insulator-to-metal transition.^{8,9} Our recent high pressure X-ray absorption experiments confirmed that a pressure-induced change of the Sm valence from the mixed $(2 + \varepsilon) +$ state at ambient conditions towards $3+$ at elevated pressures is the cause for the observed behavior.¹⁰

Isovalent and aliovalent metal substitution in the $Sm_{2.75}C_{60}$ fulleride is of great importance for the chemical control of the electronic configuration of the rare-earth ions and the tuning of their exchange interactions. Towards this direction, we have synthesized multinary $(Sm_{1-x}Ca_x)_{2.75}C_{60}$ ($x = 0 - 1$) alkaline-earth/rare-earth metal fullerides and examined the pressure evolution of the samarium valence state. We have verified the pressure-induced valence transition of the Sm ions in the whole series, while the critical pressure, the total valence change and the hysteretic loop of the valence transition strongly depend on the Ca content.¹⁰ Thus, the smallest member of this family, the $Ca_{2.75}C_{60}$ alkaline-earth metal fulleride, where the metal cations are strictly divalent, appears as a key compound for the understanding of its intriguing electronic properties under external stimuli, like pressure and temperature, and the role played by the different interfullerene separation and band filling.

Earlier electron-energy-loss spectroscopy (EELS),¹¹ as well as photoemission and inverse photoemission studies,¹² of the Ca_xC_{60} system with $x \sim 3$ showed that the t_{1u} C_{60} band is, as expected, completely filled, rendering this composition of insulating character at ambient conditions. On the other hand, Kortan *et al.* reported a superconducting phase ($T_c = 8.4$ K) for this system when $x \sim 5$.¹³ Moreover, our structural studies of $Ca_{2.75}C_{60}$ verified that the pure alkaline-earth metal fulleride shows no anomalous expansion behavior between 5 and 300 K, contrary to the situation encountered in its isostructural mixed $(Sm_{1-x}Ca_x)_{2.75}C_{60}$

compounds and compatible with the lack of an electronically active $4f$ sublattice in this case.¹⁴ Raman scattering in fullerene-based materials, which selectively probes the intramolecular C_{60} modes, is a powerful tool in the investigation of their physical properties thanks to its sensitivity to the specific molecular structural and electronic configurations and their modifications caused by external perturbations. Therefore, in this work, Raman spectroscopy, is employed to study the structural and electronic response of the $\text{Ca}_{2.75}\text{C}_{60}$ fulleride to high pressures using two pressure transmitting media that exhibit different solidification pressures and hence different hydrostatic limits.

2. Experimental Procedures

2.1. Synthesis and characterization

Polycrystalline samples with nominal composition $\text{Ca}_{2.75}\text{C}_{60}$ were prepared by direct reaction of stoichiometric quantities of C_{60} (super gold grade, > 99.9%) and calcium (dendritic pieces, Sigma Aldrich, > 99.99%). C_{60} was degassed for 15 hours at 450°C under dynamic vacuum of 10^{-5} mbar prior to synthesis, and fine Ca powder was prepared by dissolving Ca pieces using dried liquid ammonia. They were mechanically mixed and pressed into pellets, which were placed inside a tantalum (Ta) tube. The Ta tube was then sealed in a quartz tube filled with helium (~ 300 mbar) and placed in a pre-heated furnace (550°C) for 3 days with one intermediate grinding.

2.2. Structural measurements

High-resolution synchrotron X-ray diffraction experiments were carried out on the ID31 beamline at the European Synchrotron Radiation Facility (ESRF), France. The sample was sealed in a 0.5-mm diameter thin-wall glass capillary and diffraction profiles ($\lambda = 0.412740 \text{ \AA}$) were collected in continuous scanning mode at room temperature. The data were rebinned in the 2θ range $1.5\text{-}20^\circ$ to a step of 0.002° . Analysis of the diffraction data was performed with the GSAS suite of Rietveld analysis programs.

2.3. Raman measurements

Raman spectra were recorded in the back-scattering geometry using a Horiba LabRAM HR (HORIBA) spectrometer. For excitation, the 632.8 nm (785 nm in the case of the pristine C_{60} solid to avoid photo-polymerization) line of a He-Ne laser was focused on the $\text{Ca}_{2.75}\text{C}_{60}$ sample by means of a $50\times$ super long working distance (SLWD) objective, while the laser power was kept below 0.1 mW in order to eliminate any laser-heating effects. Pressure was generated by a Mao-Bell type diamond anvil cell (DAC) using the ruby fluorescence for pressure calibration while a 1:1 FC70-FC77 Fluorinert mixture or Daphne 7474 were alternatively used as the pressure transmitting medium (PTM).

3. Results and Discussion

The synchrotron X-ray diffraction profile of the $\text{Ca}_{2.75}\text{C}_{60}$ sample collected at ambient conditions is illustrated in Fig. 1. Rietveld refinement of the X-ray diffraction data confirmed the formation of an orthorhombic phase (space group $Pcab$, $R_{\text{wp}} = 12.28\%$, $R_{\text{exp}} = 8.51\%$) and yielded the structural parameters $a = 27.9160(2) \text{ \AA}$, $b = 27.9244(2) \text{ \AA}$, $c = 27.9076(2) \text{ \AA}$ and $V = 21774.8(5) \text{ \AA}^3$. As in the case of its rare-earth metal analogues ($\text{RE}_{2.75}\text{C}_{60}$), the calcium cations occupy off-centered octahedral and tetrahedral interstitial sites of the pristine fcc C_{60} lattice.^{2,6} One out of every eight tetrahedral sites is only partially occupied ($\sim 25\%$) and due to the long-range ordering of these tetrahedral Ca defects, a superstructure arises with dimensions twice as large in every direction compared to the fcc alkali fullerenes, A_3C_{60} ($\text{A} = \text{K}, \text{Rb}, \text{Cs}$).¹⁵ The structural motif of the $\text{Ca}_{2.75}\text{C}_{60}$ fulleride is depicted in Fig. 2.

In C_{60} fullerenes, the charge transfer from the metal atoms to the molecular cages, as well as the lowering of the crystal and molecular symmetry, cause frequency shifts of the Raman peaks, splitting of the fivefold degenerate H_g modes and the activation of silent — in the icosahedral molecular symmetry, I_h , of the isolated C_{60} molecule-modes.^{16,17} Hence, the Raman spectrum of the studied compound appears to be richer in structure compared to that of the pristine C_{60} solid (Fig. 3). The most prominent Raman peaks of the C_{60} solid, using the 785 nm laser line for excitation, are the $H_g(1)$ “squashing” mode and the totally symmetric $A_g(1)$ radial “breathing” and $A_g(2)$ tangential “pentagonal-pinch” modes of the C_{60} molecule. The Raman band originating from the $H_g(1)$ mode appears to split into two components at 266 and 272 cm^{-1} due to the T_h point group of the

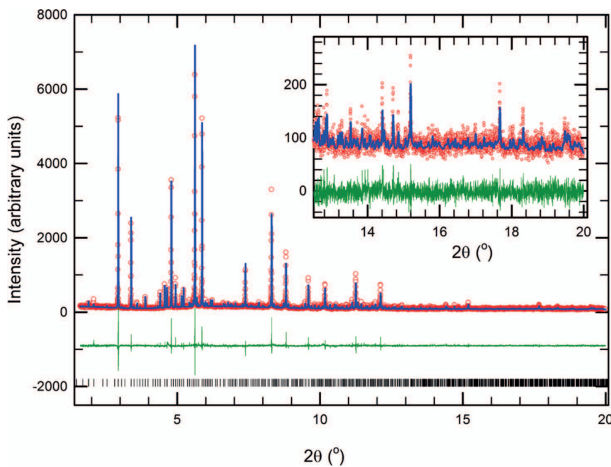


Fig. 1. (Color online) Final observed (red circles) and calculated (blue solid line) synchrotron X-ray ($\lambda = 0.412740 \text{ \AA}$) powder diffraction profiles for the $\text{Ca}_{2.75}\text{C}_{60}$ sample at ambient conditions. The lower green solid line shows the difference profiles and the tick marks show the reflection positions. The inset shows an expanded view of the diffraction profile at high Bragg angles.

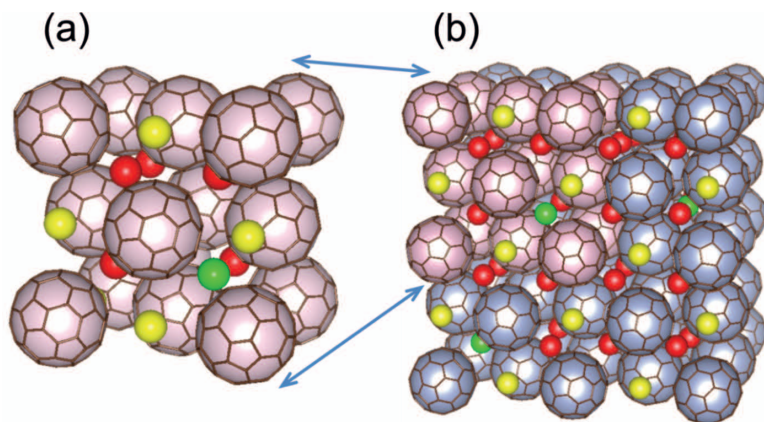


Fig. 2. (Color online) (a) Building block and (b) unit cell of the orthorhombic superstructure of $\text{Ca}_{2.75}\text{C}_{60}$ that can be obtained by doubling the subcell along all three lattice directions. Distorted octahedral and tetrahedral calcium cations are depicted as yellow and red spheres, respectively, while the tetrahedral defects are shown as green spheres.

molecules in the *fcc* phase of solid C_{60} (compatibility relation between I_h and T_h symmetry: $H_g \rightarrow E_g + T_g$).¹⁸ The corresponding band further splits in the Raman spectrum of the $\text{Ca}_{2.75}\text{C}_{60}$ fulleride into a shoulder-like peak at 265 cm^{-1} and three well-resolved peaks at 271 , 281 and 292 cm^{-1} due to the symmetry lowering.

The totally symmetric Raman modes, marked by the dashed vertical lines in Fig. 3, are located at 496 cm^{-1} $\{A_g(1)\}$ and 1468 cm^{-1} $\{A_g(2)\}$ in the C_{60} solid, in good agreement with the literature.¹⁹ In the case of $\text{Ca}_{2.75}\text{C}_{60}$, the $A_g(1)$ peak is upshifted to 509 cm^{-1} , while the $A_g(2)$ peak is downshifted to 1448 cm^{-1} . The general trend of these frequency shifts is compatible with what was previously reported for alkali, alkaline-earth and rare-earth metal fullerides. In the alkali metal fullerides, an upshift of $\sim 1\text{ cm}^{-1}$ was found for the $A_g(1)$ peak and a downshift of $6\text{--}7\text{ cm}^{-1}$ for the $A_g(2)$ peak per electron transferred from the metallic atoms to the C_{60} molecule.^{20–22} The upshift of the radial mode is attributed to the Coulomb interaction between the metal cations and the C_{60} anions while the downshift of the tangential mode to the elongation of the intramolecular bonds induced by the charge transfer process and the resulting softening of the force constants.^{16,23} In alkaline- and rare-earth metal fullerides, the frequency shifts of the totally symmetric Raman modes deviate significantly from the quasi-linear trends found in alkali metal fullerides, which is attributed to the strong metal- C_{60} coupling and their orbital hybridization.^{24–27}

The overall profile of the Raman spectrum of $\text{Ca}_{2.75}\text{C}_{60}$ appears very similar to that of $\text{Sm}_{2.75}\text{C}_{60}$, where the $A_g(1)$ and the $A_g(2)$ peak frequencies are downshifted with respect to the former compound to ~ 505 and $\sim 1441\text{ cm}^{-1}$, respectively, which cannot be explained solely by lattice size considerations.^{9,28} Moreover, it should be mentioned that the scattering efficiency and the Raman signal of the

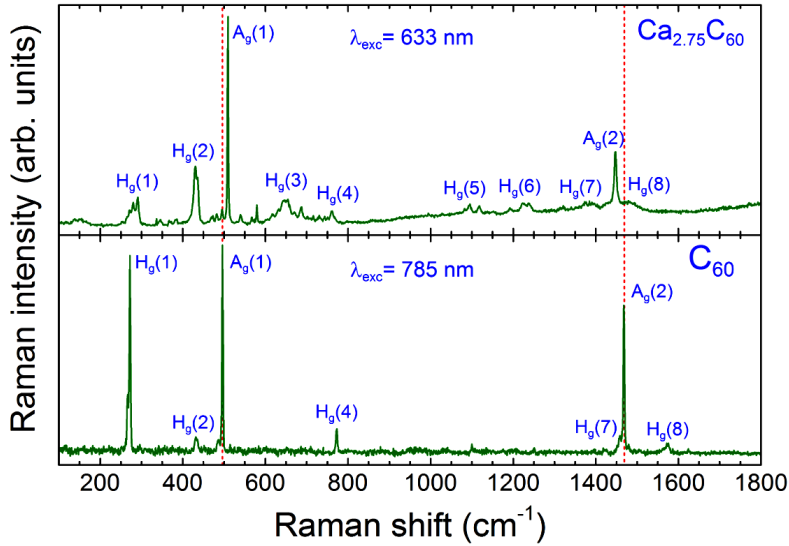


Fig. 3. (Color online) The Raman spectrum at ambient conditions of the $\text{Ca}_{2.75}\text{C}_{60}$ fulleride in comparison with that of the pristine C_{60} solid. The mode assignment refers to the irreducible representations of the C_{60} molecule in the icosahedral (I_h) symmetry. The dashed vertical lines indicate the frequency positions of the $A_g(1)$ and $A_g(2)$ Raman peaks in the pristine C_{60} .

($\text{Sm}_{1-x}\text{Ca}_x$) $_{2.75}\text{C}_{60}$ ($x = 0-1$) series increases with increasing calcium content, x ,²⁸ being compatible with the aforementioned insulating character of $\text{Ca}_{2.75}\text{C}_{60}$ at ambient conditions and indicative of a weaker metal atom- C_{60} coupling (*vide infra*).

Characteristic Raman spectra of $\text{Ca}_{2.75}\text{C}_{60}$ at various pressures recorded upon pressure increase are illustrated in Figs. 4(a) (Fluorinert mixture) and 4(b) (Daphne) for the two different pressure-transmitting media (PTM) employed in the present study. The stronger Raman signal of $\text{Ca}_{2.75}\text{C}_{60}$ has allowed us to follow also the pressure evolution of the weaker in these systems band originating from the intramolecular $A_g(2)$ mode of C_{60} , in contrast to the case of $\text{Sm}_{2.75}\text{C}_{60}$.⁹ Although the two PTM used have different solidification pressure values (~ 1 GPa for the 1:1 FC70-FC77 Fluorinert mixture and ~ 3.7 GPa for Daphne 7474),²⁹⁻³¹ the pressure evolution of the Raman spectra of the studied compound is nearly identical. Namely, the spectrum profile remains almost unaffected with increasing pressure, apart from a gradual intensity reduction of the high frequency $A_g(2)$ band, possibly originating from pressure-induced changes in the bandgap of the material and the concomitant modification of the resonant conditions. Simultaneously, the strongest Raman peaks shift to higher frequencies, in accordance with the commonly expected hardening of the intramolecular bonds with pressure.

The pressure dependence of the frequencies, ω , of the well-resolved Raman peaks of $\text{Ca}_{2.75}\text{C}_{60}$ is illustrated in Fig. 5, where the corresponding pressure coefficients,

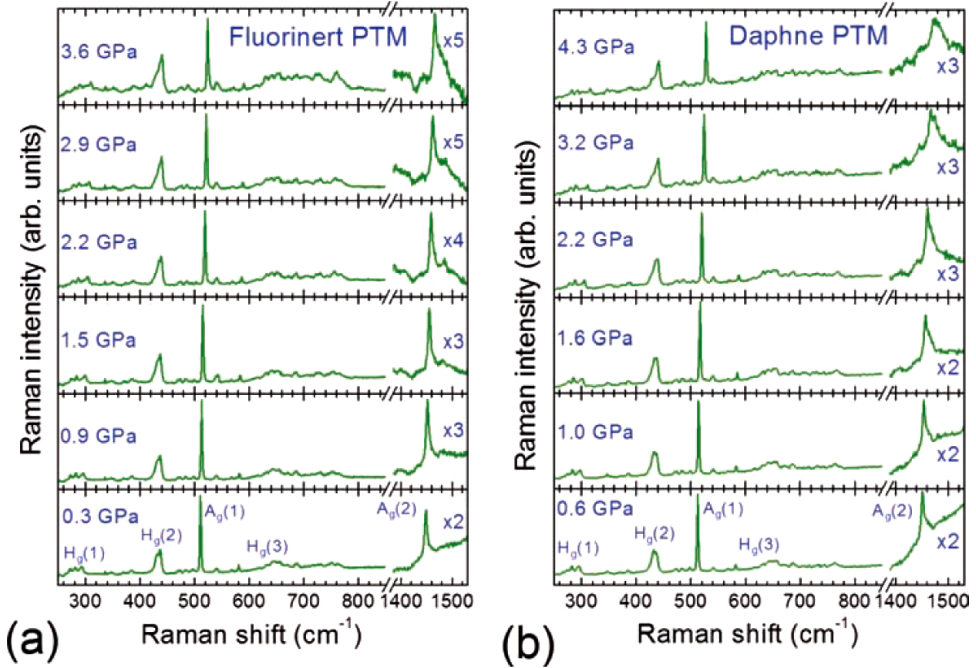


Fig. 4. (Color online) Characteristic Raman spectra of $\text{Ca}_{2.75}\text{C}_{60}$ at various pressures using (a) 1:1 FC70-FC77 Fluorinert mixture and (b) Daphne 7474 as the pressure transmitting medium. The mode assignment refers to the irreducible representations of the C_{60} molecule in the I_h symmetry.

$\partial\omega/\partial P$, are also given. The pressure induced frequency shifts are quasi-linear in the whole pressure region investigated and fully reversible upon pressure release, as indicated by the solid symbols in the figure, suggesting the structural stability of the material up to the maximum pressure attained in the present experiments (~ 4.5 GPa). As it was mentioned above, the pressure coefficients of all the studied Raman peaks are positive with the only exception being that of the low intensity peak at ~ 687 cm^{-1} , attributed to the $H_g(3)$ mode of the C_{60} molecule, which has a small negative value. This negative pressure coefficient is reminiscent of those observed in the case of the pristine C_{60} fullerene for peaks attributed to the $H_g(3)$ and $H_g(4)$ intramolecular modes.^{32,33} Moreover, as it can be inferred from Fig. 5, the pressure coefficients of the corresponding Raman peaks are practically, within the experimental accuracy, the same for the two different PTM employed in this study.

The values of the pressure coefficients for all the Raman peak frequencies of $\text{Ca}_{2.75}\text{C}_{60}$ lie closely to the corresponding ones obtained for solid C_{60} and are larger, in general, than those found for the isostructural $\text{Sm}_{2.75}\text{C}_{60}$ compound.^{9,34} More specifically, the totally symmetric $A_g(1)$ and $A_g(2)$ intramolecular modes exhibit in the C_{60} solid pressure coefficient values of 4.2 and 5.5 $\text{cm}^{-1}\text{GPa}^{-1}$, respectively,³⁴

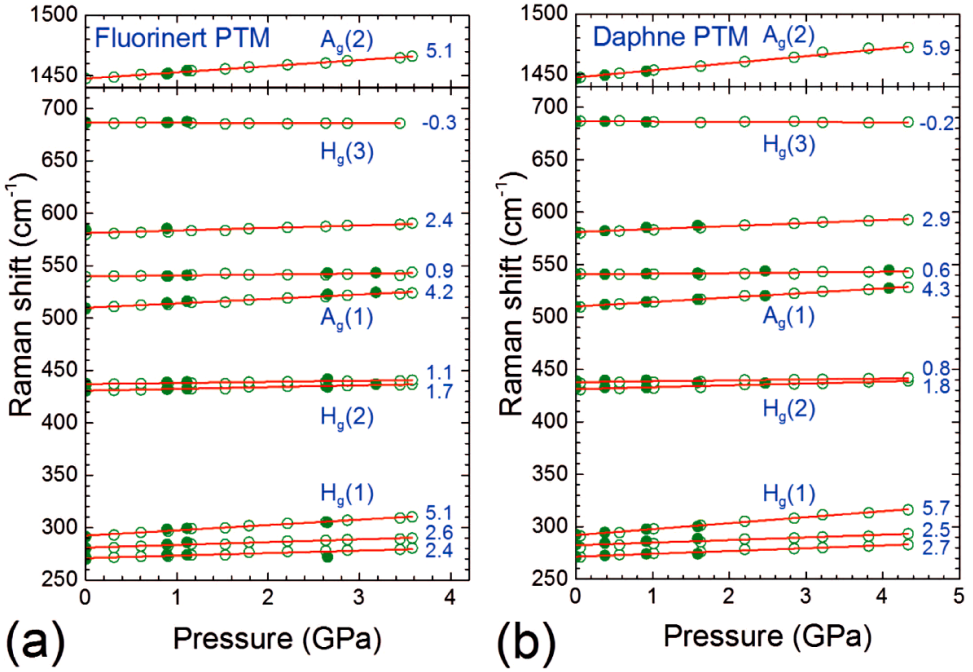


Fig. 5. (Color online) Pressure dependence of well-resolved Raman peak frequencies of $\text{Ca}_{2.75}\text{C}_{60}$ using (a) 1:1 FC70-FC77 Fluorinert mixture and (b) Daphne 7474 as the pressure transmitting medium. Numbers on the right of each panel refer to their pressure coefficients in $\text{cm}^{-1}\text{GPa}^{-1}$, obtained from linear least-squares fits to the experimental data (solid lines through the symbols). Open (solid) symbols denote data obtained upon pressure increase (decrease). The mode assignment refers to the irreducible representations of the C_{60} molecule in the I_h symmetry.

being essentially identical to those in $\text{Ca}_{2.75}\text{C}_{60}$. On the other hand, in $\text{Sm}_{2.75}\text{C}_{60}$ the pressure coefficient of the peak originating from the $A_g(1)$ radial breathing mode deviates significantly from these values, being only $2.6 \text{ cm}^{-1}\text{GPa}^{-1}$.⁷ The much smaller value in this case has been ascribed to the reduced compressibility of the rare-earth metal fulleride,⁸ compared with that of the pristine C_{60} ,³⁵ and the strong Sm- C_{60} coupling.⁹ Therefore, our findings are compatible with a weaker Ca- C_{60} coupling and orbital mixing in the case of the $\text{Ca}_{2.75}\text{C}_{60}$ fulleride.

4. Conclusions

In summary, pure $\text{Ca}_{2.75}\text{C}_{60}$ alkaline-earth metal fulleride was isolated and structurally characterized by synchrotron X-ray powder diffraction. The analysis of the X-ray diffraction data reveals that $\text{Ca}_{2.75}\text{C}_{60}$ adopts an orthorhombic structure, which is similar to that of the rare-earth metal C_{60} fullerides having the same composition. The pressure response of $\text{Ca}_{2.75}\text{C}_{60}$ was examined by means of Raman spectroscopy. Two different fluids were employed as PTM, providing almost identical results and thus confirming the reproducibility of our findings. The pressure

evolution of the Raman spectrum, the quasi-linear pressure dependence and the reversibility of the Raman peak frequencies demonstrate the stability of the studied compound for pressures up to 4.5 GPa and is in line with the robust divalent state of the metal cations. The pressure coefficients of the peaks originating from the totally symmetric $A_g(1)$ and $A_g(2)$ modes of the C_{60} molecule are practically identical to those of the pristine C_{60} solid. This finding along with the much larger pressure coefficient of the $A_g(1)$ peak frequency in $\text{Ca}_{2.75}\text{C}_{60}$ compared to that in its isostructural $\text{Sm}_{2.75}\text{C}_{60}$ analogue is suggestive of a weaker coupling between the metal cations and the C_{60} anions in the case of the studied alkaline-earth metal fulleride.

Acknowledgments

We thank the ESRF for the access to synchrotron X-ray facilities as well as the Center of Interdisciplinary Research and Innovation of the Aristotle University of Thessaloniki (CIRI-AUTH), Greece for the access to the Raman instrumentation. AGVT acknowledges the support by the Hellenic Foundation for Research and Innovation (HFRI) under the HFRI PhD Fellowship grant (Fellowship Number: 707). This work was financially supported by Grants-in-Aid for Scientific Research (JSPS KAKENHI Grant Numbers JP18H04303, JP18K18724, and JP19H04590) by the Ministry of Education, Culture, Sports, Science and Technology (MEXT), Japan and by the KAKENHI Specific Support Operation of Osaka Prefecture University.

References

1. S. Margadonna *et al.*, *Struct. Bonding* **109** (2004) 127.
2. J. Arvanitidis *et al.*, *Nature* **425** (2003) 599.
3. Y. Takabayashi and K. Prassides, *Struct. Bonding* **172** (2016) 119.
4. M. Menelaou *et al.*, *Int. J. Mod. Phys. B* **32** (2018) 1840020.
5. H. E. Okur and K. Prassides, *J. Phys. Chem. Solids* **131** (2019) 44.
6. S. Margadonna *et al.*, *Chem. Mater.* **17** (2005) 4474.
7. A. Jayaraman *et al.*, *Phys. Rev. Lett.* **25** (1970) 1430.
8. J. Arvanitidis *et al.*, *Dalton Trans.* (2004) 3144.
9. S. M. Souliou *et al.*, *High Pres. Res.* **31** (2011) 13.
10. N. Yoshikane *et al.*, in preparation (2020).
11. H. Romberg *et al.*, *Phys. Rev. B* **49** (1994) 1427.
12. Y. Chen *et al.*, *Phys. Rev. B* **46** (1992) 7961.
13. R. Kortan *et al.*, *Nature* **355** (1992) 529.
14. K. Prassides *et al.*, *Phil. Trans. R. Soc. A* **366** (2008) 151.
15. R. H. Zadik *et al.*, *Sci. Adv.* **1** (2015) e1500059.
16. P. Zhou *et al.*, *Phys. Rev. B* **46** (1992) 2595.
17. H. Kuzmany and B. Burger, *J. Mol. Struct.* **347** (1995) 39.
18. M. S. Dresselhaus *et al.*, *Science of Fullerenes and Carbon Nanotubes* (Academic Press, San Diego, 1996), p. 99.
19. Z. H. Dong *et al.*, *Phys. Rev. B* **48** (1993) 2862.
20. J. Winter and H. Kuzmany, *Solid State Commun.* **84** (1992) 935.
21. H. Kuzmany *et al.*, *Adv. Mater.* **6** (1994) 731.

A. G. V. Terzidou *et al.*

22. M. Kosaka *et al.*, *Phys. Rev. B* **59** (1999) R6628.
23. R. A. Jishi and M. S. Dresselhaus, *Phys. Rev. B* **45** (1992) 6914.
24. X. H. Chen *et al.*, *Phys. Rev. B* **60** (1999) 12462.
25. J. Arvanitidis *et al.*, *Nanoscale* **3** (2011) 2490.
26. B. Gogia *et al.*, *Phys. Rev. B* **58** (1998) 1077.
27. C. M. Brown *et al.*, *Phys. Rev. Lett.* **83** (1999) 2258.
28. T. Nakagawa *et al.*, *AMIS2017 — The AIMR International Symposium 2017* (Sendai, 2017).
29. S. Sasaki *et al.*, *Jpn J. Appl. Phys.* **49** (2010) 106702.
30. N. Tateiwa and Y. Haga, *Rev. Sci. Instrum.* **80** (2009) 123901.
31. V. Sidorov and R. Sadykov, *J. Phys.: Condens. Matter* **17** (2005) S3005.
32. K. P. Meletov *et al.*, *Phys. Rev. B* **52** (1995) 10090.
33. B. Sundqvist, *Adv. Phys.* **48** (1999) 1.
34. K. P. Meletov *et al.*, *J. Exp. Theor. Phys.* **81** (1995) 798.
35. S. J. Duclos *et al.*, *Nature* **351** (1991) 380.